Empirical rule to reconcile BCS theory with electron-phonon interaction in normal state

Empirical rule to reconcile Bardeen–Cooper–Schrieffer theory with electron–phonon interaction in normal state

2014 Phys. Scr. 89 095803

(http://iopscience.iop.org/1402-4896/89/9/095803)

OPEN ACCESS

Made open access 05 January 2015

IOP Publishing | Royal Swedish Academy of Sciences

Physica Scripta

Phys. Scr. **89** (2014) 095803 (9pp)

doi:10.1088/0031-8949/89/9/095803

Empirical rule to reconcile Bardeen–Cooper–Schrieffer theory with electron–phonon interaction in normal state

X H Zheng and D G Walmsley

Department of Physics and Astronomy, Queen's University of Belfast, Belfast, BT7 1NN, UK

E-mail: xhz@qub.ac.uk and dg.walmsley@qub.ac.uk

Received 10 December 2013, revised 28 May 2014
Accepted for publication 18 June 2014
Published 25 July 2014

Abstract

We introduce a simple empirical rule wherein the pairing interaction in superconductors is cancelled when normal and umklapp phonon scattering coexist. Superconductivity then arises solely from the residual umklapp contribution. As a result the deduced electron–phonon interactions in niobium, tantalum, lead and aluminum become virtually identical in the normal and superconducting states. Transition temperatures calculated under the rule are accurate within a few per cent when compared with experimental data. Features of the Matthias relations are also explained. The high T_c so far predicted for metallic hydrogen is probably overly optimistic.

Keywords: superconductivity, BCS theory, T_c prediction, Matthias relations

1. Introduction

In 1957 Bardeen, Cooper and Schrieffer (BCS) published the first successful and remarkably comprehensive microscopic theory of superconductivity [1]. It raised the hope that some day we might be able to understand and predict accurate numerical values for the superconducting transition temperature, T_c [2]. More than 50 years on the goal still eludes us [4, 3]. Now is perhaps the time to seek some pragmatic progress.

We recall that in the 1970s and 1980s a number of attempts were made to calculate the superconducting electron–phonon spectral density, $\alpha^2F(\nu)$, which leads to T_c via numerical calculation within the Eliashberg–Nambu formalism, a refined version of the BCS theory, see [5, 6] and the references therein. Meanwhile, apparently as a check, attempts were made to calculate electrical resistivity against temperature, $\rho(T)$, which derives from the same electron–phonon interaction in the normal state. Scrutiny shows that the outcome was a consistent mismatch: either $\alpha^2F(\nu)$ was too strong when $\rho(T)$ was reasonable [7–9], or $\alpha^2F(\nu)$ was reasonable but $\rho(T)$ was too weak [10–13]. A similar observation was reported in the 1990s, with $\rho(T)$ largely reasonable but $\alpha^2F(\nu)$ exceeding experimental values by a factor 2 or 3 in places [14].

In the current literature the McMillan formula, or a variation of it, is often used in making a rough estimate of T_c [15–22]. Sometimes a novel density functional theory of the superconducting state has been attempted [23–26]. In general the outcome is roughly right but, to our knowledge, control measures are not taken to verify consistency with $\rho(T)$ calculated for the normal state. Rather surprisingly and remarkably the theoretical $\alpha^2F(\nu)$ determined in [14] also leads through the density functional theory to tolerably acceptable T_c (error ~25%) [24].

Recently we developed a technique to extract realistic effective atomic potentials (pseudopotentials) for superconductive metals [27]. In a further development we also extracted atomic potentials in the same metals in the normal state and determined that the potentials have to be consistently much stronger in the normal than in the superconducting state if they are to account for $\rho(T)$, at least for the elements tantalum, niobium, lead and aluminum [28]. The relative weakness of the effective atomic potential in the superconductive state is so significant that little room is left for an explanation in terms of observational or numerical inaccuracies.

It seems implausible that the actual strength of the atomic potential can be weakened significantly in the transition to the superconducting state. As a pragmatic measure, we propose an empirical rule to resolve the problem, a treatment which is plausible but without generally accepted underlying theoretical justification as yet. Our proposal is that the electron–phonon interaction ceases to contribute to superconductivity when normal and umklapp scattering coexist. We describe the

situation as normal and umklapp scattering events cancelling each other. Under our empirical rule superconductivity arises solely from residual uncancelled umklapp scattering.

As before, we test our treatment with niobium, tantalum, lead and aluminum. Starting with experimental values of $\rho(T)$ we find the atomic potential that leads to these values using the method of inversion of Hooke and Jeeves [29]. This achieves a highly accurate relation between the potential and the values of $\rho(T)$ over a wide range of T. The inversion is formulated on the established theory of electrical resistivity, with no further assumption or approximation. The resultant atomic potential is therefore hardly more than reformulated experimental $\rho(T)$ data. Next we invert the experimental superconducting tunnelling conductance data, $\sigma(\omega)$, with a similar technique but include the empirical rule of normal-umklapp cancellation. The resultant atomic potential is again hardly more than reformulated experimental data.

The value of an empirical rule lies chiefly in its ability to reconcile theory and experiment and hence validate the theory for prediction. To this end we compare the atomic potentials we have found in the normal and superconducting states. The outcome supports the validity of the empirical rule. For additional support of our empirical rule we provide a short clear proof of an algebraic contradiction of the pairing scheme when normal and umklapp scattering coexist. It manifests a proven theoretical result valid in the original BCS theory [30–32]. We also compare calculated T_c values with experiment.

This article is arranged as follows: in sections 2 and 3 we detail a dilemma due to umklapp scattering and the empirical rule to deal with it. In section 4 we invert electric resistivity data for niobium. In section 5 we invert tunnelling conductance data for niobium. In section 6 we study tantalum, lead and aluminum. In section 7 we calculate T_c theoretically for the four metals. We discuss the Matthias relations and metallic hydrogen in section 8. A brief summary and conclusions are given in section 9.

2. Umklapp dilemma

Throughout our discussion we assume a spherical electron Fermi surface of radius k_F, shown schematically in figure 1 as an open circle. Let $\mathbf{k}$ and $-\mathbf{k}$ be the initial momenta of a pair of electrons on the Fermi surface and $\mathbf{k}'$ and $-\mathbf{k}'$ their end momenta after being scattered by phonons. In figure 1 we mark the range of scattering with the grey wedges. In the Debye model the first phonon Brillouin zone is simplified to a sphere of radius q_D. We have $q_D/2k_F = (1/4Z)^{1/3}$, k_F and q_D are Fermi and Debye wavenumbers, respectively, Z is valency, giving $\theta = 2\sin^{-1}(q_D/2k_F)$ as the angle of the wedges against their symmetric axis, $\theta = 78.1°, 60.0°, 51.8°, 46.8°$, ... when $Z = 1, 2, 3, 4$, ... With realistic phonons the phonon zone becomes polyhedral and θ will depend on $\mathbf{q} = \mathbf{k}' - \mathbf{k}$ though not significantly.

Consider umklapp scattering. For definitiveness we will consider phonons in the first Brillouin zone but place the electrons in periodical zones. In figure 1 we use a partial circle

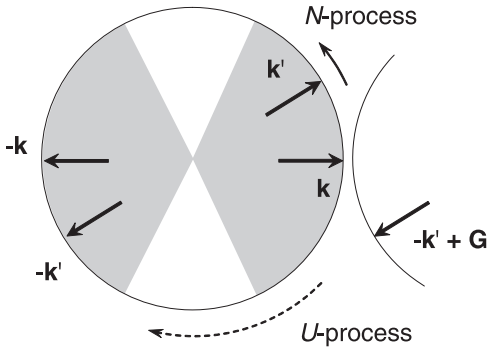

Figure 1. Schematic of a spherical Fermi surface and a pair of electrons with initial momenta $\mathbf{k}$ and $-\mathbf{k}$. Normal scattering drives the electrons into $\mathbf{k}'$ and $-\mathbf{k}'$ within the grey wedges. It can also drive an electron from $\mathbf{k}$ to $-\mathbf{k}' + \mathbf{G}$ in the neighbouring Brillouin zone, that is $-\mathbf{k}' = (-\mathbf{k}' + \mathbf{G}) - \mathbf{G}$ is also accessible via umklapp scattering.

to represent a replica of the Fermi surface in one of the neighbouring electron zones. Apparently a state on this replicated Fermi surface, for example $-\mathbf{k}' + \mathbf{G}$, is accessible via normal electron–phonon scattering, if it is not too far away from the initial state, $\mathbf{k}$, where $\mathbf{G}$ is a crystal momentum vector. This means that we have an alternative path to access $-\mathbf{k}'$, namely umklapp scattering, since $-\mathbf{k}' + \mathbf{G}$ is just a replica of $-\mathbf{k}'$.

Now we have a dilemma: let $h(\mathbf{k}')$ and $h(-\mathbf{k}')$ be pair occupancy probabilities at $\mathbf{k}'$ and $-\mathbf{k}'$ [1]. By symmetry of the pairing scheme $h(\mathbf{k}')$ and $h(-\mathbf{k}')$ must be equal. On the other hand $h(\mathbf{k}')$ and $h(-\mathbf{k}')$ arise from normal and umklapp scattering, respectively, so that they need not and in general will not be equal. This is a manifestation of the algebraic contradiction within the original BCS theory [30–32] that the ground state electronic wavefunction cannot be normalized when normal and umklapp scattering coexist, see appendix.

Study of umklapp scattering in the BCS theory has a long history. In 1958 Pines calculated normal and umklapp contributions to the original BCS theory [33]. In 1968 Carbotte and Dynes calculated umklapp contributions to the Eliashberg–Nambu formalism by enlarging the radius of the sphere enveloping available phonons to $2k_F$, so that the entire Fermi surface is within the reach of an initial electron scattered by phonons [34]. We carried out a numerical test and checked that electrons from umklapp scattering do arrive everywhere over the Fermi surface if the phonon zone is not spherical but a realistic polyhedron. We also find the end states of normal and umklapp scattering never overlap. Both fcc and bcc lattices have been tested with valencies, Z, between 1 and 4.

3. Empirical rule

To avoid the umklapp dilemma we propose an empirical rule. In figure 2 we show the range of normal and umklapp scattering when $\mathbf{q}$ is in a specific direction, $\mathbf{q} = \mathbf{k}' - \mathbf{k}$ being the phonon momentum vector. For Debye phonons $\omega = v_D q$, $0 \leqslant q \leqslant q_D$, where ω is the phonon frequency, v_D

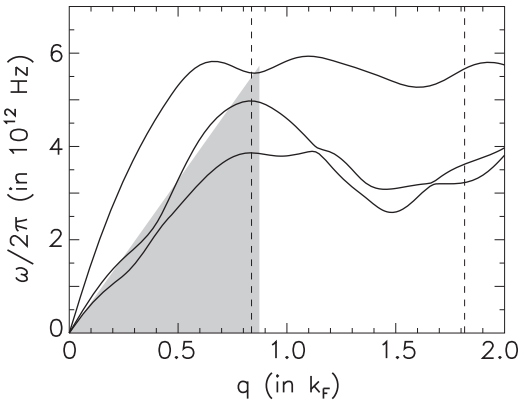

Figure 2. Nb phonon dispersion in the (0.884, 0.451, 0.123) direction, grey triangle envelops Debye frequencies and momenta, dashed vertical lines mark the ranges of normal electron–phonon scattering for the two electrons in a pair, respectively. Under the empirical rule superconductivity arises solely with q between the two dashed lines.

sound velocity and $q = |\mathbf{q}|$. We use the grey triangle to mark the ranges of both ω and q in the Debye model, corresponding to the right grey wedge of figure 1. If the value of q exceeds

$$\sqrt{4k_F^2 - q_D^2} \tag{1}$$

then an electron, initially with momentum $\mathbf{k}$, enters the grey wedge on the left side of figure 1 via umklapp scattering. Over the range of this wedge each and every electron state can also be accessed via normal scattering of the electron initially with momentum $-\mathbf{k}$. In figure 2 we use the dashed vertical line on the left to mark the actual boundary of the first Brillouin zone, which is slightly different from q_D. We use the dashed line on the right to mark the value of expression (1), when $\mathbf{q}$ is in the direction concerned, with q_D being replaced by the actual value of the Brillouin zone boundary in that direction.

According to the proposed empirical rule normal and umklapp electron–phonon scattering, with end states of the electrons in the grey wedges in figure 1, cancel each other with respect to their contributions to superconductivity. A metal becomes a superconductor solely on account of residual umklapp scattering that drives electrons into the range between the two grey areas. Correspondingly in figure 2 only phonons between the two dashed lines make contributions to superconductivity. We disregard other phonons when we evaluate $\alpha^2F(\nu)$.

4. Resistivity: niobium

According to Mott and Jones, contributions of normal and umklapp scattering to electrical resistivity in the normal state are simply added together [35]. Previously we have found the atomic potential in the normal state by inversion of the temperature-dependent electrical resistivity, $\rho(T)$ [28]. Here we describe the work briefly, with some insights, for the convenience of the reader. Drude theory has a number of refined versions, often with the formula [13]

$$\frac{1}{\tau} = 4\pi\frac{k_BT}{\hbar}\int_0^\infty \frac{\alpha_{\rm tr}^2F(\nu)x\mathrm{d}x}{\left(e^x-1\right)\left(1-e^{-x}\right)} \tag{2}$$

to estimate the collision time (relaxation time), which measures the average time between electron collisions with the atoms, where $x = \nu/k_BT$, ν being the phonon frequency in electron volts, k_B Boltzmann constant and T temperature. When the Fermi surface is spherical, the so-called transport spectral density can be written into the following programmable form [28]:

$$\alpha_{\rm tr}^2F(\nu) = \frac{3}{4}\left(\frac{2}{Z}\right)^{2/3}\frac{m}{M}\left(\frac{T_F}{T_D}\right)^2 \times\frac{1}{2\pi}\int_0^{2\pi}\mathrm{d}\phi\sum_\ell\frac{\mathbf{k}\cdot\mathbf{q}}{k_Fq_D}e_\ell^2\frac{\omega}{\omega_\ell}\frac{\mathrm{d}\omega}{\mathrm{d}\omega_\ell}\left[\frac{q}{q_D}\frac{V(q)}{\epsilon_F}\right]^2_{\hbar\omega_\ell=\nu} \tag{3}$$

with m and M being electronic and atomic mass, T_F and T_D Fermi and Debye temperatures, $\mathbf{k}$ initial vector momentum of the electron, $\mathbf{q}$ phonon momentum vector, k_F and q_D Fermi and Debye momentum, $\ell = 1, 2, 3$ identifies phonon polarization, $e_1^2 + e_2^2 + e_3^2 = 1$, $\omega_\ell = \omega_\ell(\mathbf{q})$ angular phonon frequency, $V(q)$ atomic potential in reciprocal space and ϵ_F Fermi energy.

In equation (3) the variable ν determines the phonon frequency via the relation $\hbar\omega_\ell(\mathbf{q}) = \nu$ which in turn determines $\mathbf{q}$ via the phonon dispersion relation. We notice that in equation (3) each and every value of ϕ defines a great circle across the Fermi sphere, which is a trace of the end state, $\mathbf{k}'$, of the electron being scattered. In order to evaluate equation (3) we trace this great circle until $\mathbf{q} = \mathbf{k}' - \mathbf{k}$ takes the value determined by ν. Consequently, when ϕ runs between 0 and 2π, we find a range of $\mathbf{q}$ to evaluate the integrand in equation (3). An average of the evaluated integrand over ϕ leads to $\alpha_{\rm tr}^2F(\nu)$.

In practice we let $\mathbf{q}$ in equation (3) run over all possible values of phonon momentum or, equivalently, within the 1/48 irreducible section of the phonon sphere. Following Mott and Jones the radius of the phonon sphere is $2k_F$ to include umklapp scattering [35]. In our calculation $\mathbf{q}$ has 250 values in each of 1275 directions, so that we have to solve 318750 eigen-equations for 956 250 phonon frequencies. In doing so we find a spectrum of ν via the relation $\nu = \hbar\omega_\ell(\mathbf{q})$. This relation is not linear so values of ν may cluster together. Meanwhile we evaluate the integrand in equation (3) with the values of $\mathbf{q}$ and $\omega_\ell(\mathbf{q})$. An average of the evaluated integrand, with respect to ϕ, leads to $\alpha_{\rm tr}^2F(\nu)$. We encounter a peak of $\alpha_{\rm tr}^2F(\nu)$ whenever values of ν cluster together. This common practice deviates slightly from the physics, because apparently we have to exclude a lot of phonons in order to land the electron nowhere else but just on the Fermi surface. We did a numerical test to simulate electron–phonon scattering on the Fermi surface to the letter. We found little improvement at the cost of a much higher amount of computation.

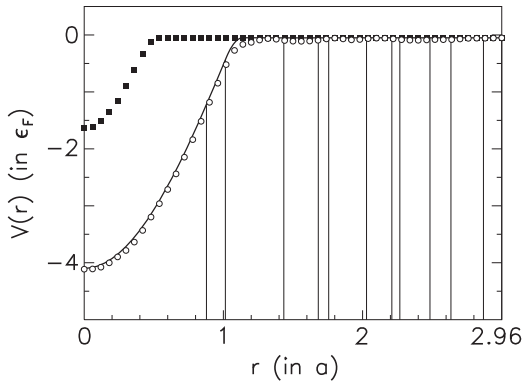

Figure 3. Atomic potentials extracted from Nb in the normal state (continuous curve) and superconducting state with (open circles) and without (filled squares) normal-umklapp cancellation; vertical lines mark neighboring atomic shells.

In equation (3) $V(q)$ is found from Fourier transformation of its counterpart in real space, $V(r)$. We start inversion of the electrical resistivity data with the following muffin tin pilot potential:

$$V(r) = \delta V \cos\left(\frac{\pi r}{2r_1}\right) \tag{4}$$

when $0 \leqslant r \leqslant r_1$, otherwise $V(r) = 0$, r being the distance from the atomic site. With a simple procedure of optimization we adjust δV and r_1 until the electric resistivity from equations (2–4) best matches experimental data. This takes place when $\delta V = -4.10\epsilon_F$ and $r_1 = 1.06a$, a being the crystal constant. We then further adjust $V(r)$ on 24 values of r with intermediate values found via interpolation using second order polynomials. In the pattern search phase of the Hooke–Jeeves procedure [29] the 24 values of $V(r)$ are perturbed in turn. Perturbations are registered as favorable when theoretical and experimental resistivity data, $\rho(T)$, fit better. In the pattern move phase of the procedure favorable perturbations are implemented, unfavorable perturbations implemented in the opposite directions, all simultaneously by an amount appropriate to optimize the fitting. This process is iterated until a satisfactory fit has been reached. The resultant $V(r)$, shown as the continuous curve in figure 3, differs little from the pilot potential.

In the upper part of figure 4 we present, as a continuous curve, the analytical expression of $\rho(T)$ for Nb, given by Webb [37] to fit his experimental data. We present the calculated $\rho(T)$ from equations (2–4) as open circles. On average the difference between experiment and theory is just 0.12% relative to ρ at 295 K. In the lower part of figure 4 we present the related transport spectral density, $\alpha^2_{\rm tr}F(\nu)$, as a histogram. In the Bloch–Grüneisen formula $\alpha^2_{\rm tr}F(\nu)$ is reduced to $8.95x^4$ when $x \leqslant 1$ (= 0 when $x > 1$), with $x = \nu/k_B\Theta$, $\Theta = 270$ K [36]. It is presented in the lower part of figure 4 as the grey silhouette.

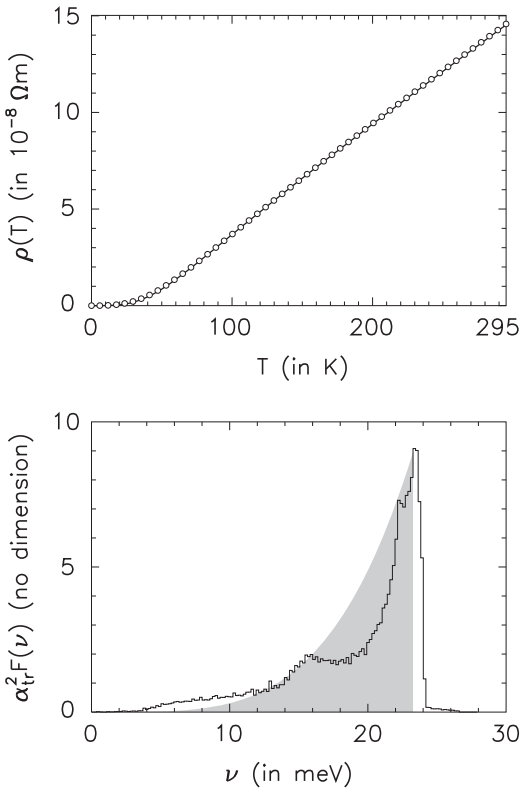

Figure 4. Upper: measured (continuous curve) and computed (open circles) normal state resistivity of Nb. Lower: normal state electron–phonon spectral density, $\alpha^2_{\rm tr}F(\nu)$, in Nb (histogram) and its counterpart in the Grüneisen–Bloch formulation (grey silhouette).

5. Superconductivity: niobium

The superconducting electron–phonon spectral density can be written into the following programmable form [28]:

$$\alpha^2F(\nu) = \frac{3}{4}\left(\frac{2}{Z}\right)^{1/3}\frac{m}{M}\left(\frac{T_F}{T_D}\right)^2 \times\frac{1}{2\pi}\int_0^{2\pi} d\phi \sum_\ell e_\ell^2 \frac{\omega}{\omega_\ell}\frac{d\omega}{d\omega_\ell}\left[\frac{q}{q_D}\frac{V(q)}{\epsilon_F}\right]^2_{\hbar\omega_\ell = \nu} \tag{5}$$

which is very similar to equation (3) and leads through the Eliashberg–Nambu equations [6] to the superconducting energy gap function, $\Delta(\omega)$, which in turn leads to the theoretical quasiparticle density of states, $\sigma(\omega)$, the real part of the expression $\omega/[\omega^2 - \Delta^2(\omega)]^{1/2}$. This will be reduced to $\sigma_{\rm BCS}(\omega)$ if $\Delta(\omega)$ is replaced with the gap edge, Δ_0 [38]. The quantity $\sigma/\sigma_{\rm BCS}$ reveals phonon structure and serves as the major theoretical output to be compared with its experimental counterpart, similar to $\rho(T)$ in section 4. In this paragraph and figure 5 we use ω to represent the electronic wave frequency (in eV), which should not be confused with the phonon frequency (in rad s^{-1}) in equations (3) and (5).

Previously we inverted the experimental data of Khim, Burnell and Wolf [40] without normal-umklapp cancellation [28]. We describe some details of the work for easy comparison with the new result. We started with the pilot potential in equation (4), $r_1 = 0.46a$ and $\delta V = -1.62\epsilon_F$. We adjusted

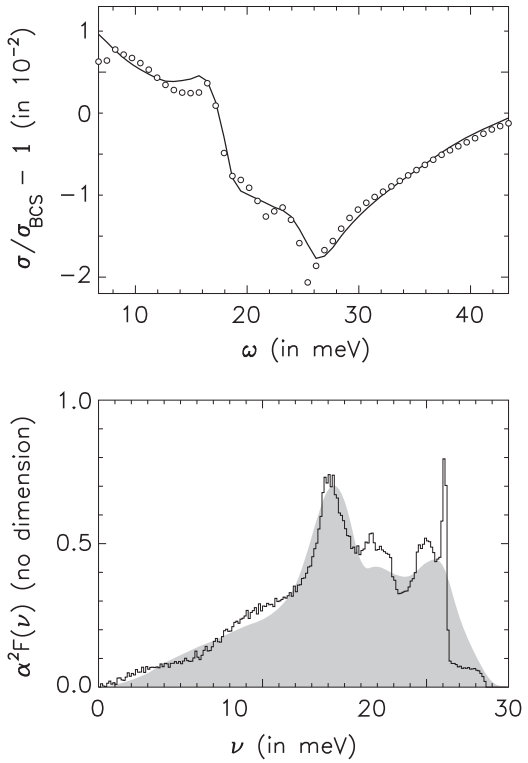

Figure 5. Upper: normalized superconducting tunneling quasiparticle density of states in Nb. The continuous curve is experimental, open circles are from inversion with normal-umklapp cancellation, ω stands for electron frequency. Lower: superconducting electron–phonon spectral density, $\alpha^2F(\nu)$, the grey silhouette and histogram are associated with the continuous curve and circles in the upper part respectively.

24 values of $V(r)$ when $0 < r \leqslant 2.96a$ in both the pattern search phase and pattern move phase of inversion. The procedure was iterated a number of times and eventually we found $V(r)$ represented by the filled squares in figure 3, which is much weaker than $V(r)$ for the normal state (continuous line).

Now, under the proposed empirical rule, we again extract $V(r)$ with normal-umklapp cancellation included. We evaluate $\alpha^2F(\nu)$ in equation (5) only with phonons between the two dashed lines in figure 2. In practice, we assign 1275 directions within the irreducible section of the phonon sphere. We let $\mathbf{q}$ run along each of these directions. We evaluate the integrand in equation (5) when $q_B(\mathbf{q}) < q < [4k_F^2 - q_B^2(\mathbf{q})]^{1/2}$, $q_B(\mathbf{q})$ being the realistic radius of the first phonon Brillouin zone in the direction of $\mathbf{q}$, in accord with equation (1). Values of the integrand are arranged as a function of ν and stored. An average of these functions, with respect to the number of directions of $\mathbf{q}$, leads to $\alpha^2F(\nu)$ with normal-umklapp cancellation. It is then straightforward to find $V(r)$ from $\alpha^2F(\nu)$ via the inversion procedure.

We pilot the inversion with the Muffin-tin potential in equation (4), with $\delta V = -4.10\epsilon_F$ and $r_1 = 1.06a$, the same potential we used to pilot normal state inversion. Further refinement of this pilot potential, by varying $V(r)$ at 24 values of r, leads to the open circles in figure 3. On average the difference between these circles and the continuous line arising from $\rho(T)$ inversion in figure 3 is 0.65% relative to the depth of the potential. In the upper part of figure 5 we show the calculated and experimental normalized quasiparticle densities of states. In the lower part of figure 5 we show as the histogram $\alpha^2F(\nu)$ calculated enroute inversion with normal-umklapp cancellation. We also show as the grey silhouette the experimental $\alpha^2F(\nu)$ found from the data in [40] by the original method of McMillan and Rowell [38].

The atomic potential in figure 3 is often known as a pseudopotential. Received opinion is that such a pseudopotential is 'not unique nor exact, but it may be very good' [39]. Choices other than equation (4) are available to pilot inversion of experimental $\rho(T)$ or $\sigma(\nu)$: square well, empty core or Gaussian. Trying them we find somewhat different $V(r)$ with albeit similar depth at $r = 0$. However in our experience, for the case of niobium, the Muffin-tin potential in equation (4), with the abovementioned values of δV and r_1, best achieves the almost exact compatibility in figure 3 between values of $V(r)$ in the normal and superconducting states. It seems now that, crosschecking between normal and superconducting states, we are able to pin down a unique $V(r)$ for the electron–phonon interaction in niobium perhaps for the first time.

6. Tantalum, lead and aluminum

In the case of tantalum in the normal state, for which there is no experimental data readily available, we invert $\rho(T)$ from the Bloch–Grüneisen formula, $\Theta = 228$ K [36]. We let $\delta V = -4.49\epsilon_F$ and $r_1 = 1.07a$ in equation (4) to pilot normal state inversion. Further optimization, via the procedure of Hooke and Jeves [29], entails little change to the pilot potential, giving $V(r)$ shown in the upper part of figure 6 as the continuous curve. In the superconducting state we invert the experimental tunneling data of Wolf *et al* [41]. Without normal-umklapp cancellation we let $\delta V = -1.81\epsilon_F$ and $r_1 = 0.47a$ in equation (4) to pilot superconducting state inversion. Further optimization leads to a weak potential represented by the filled squares in figure 6. With normal-umklapp cancellation we let $\delta V = -4.50\epsilon_F$ and $r_1 = 1.08a$ in equation (4) to pilot inversion and eventually find the potential represented by open circles in the upper part of figure 6. On average we have a difference of 1.29%, relative to the depth of the potential well, between the values of $V(r)$ found for the normal state (continuous curve) and superconducting state with formal normal-umklapp cancellation (open circles).

Again, in the case of lead in the normal state we invert $\rho(T)$ from the Bloch–Grüneisen formula, $\Theta = 86$ K [36]. We let $\delta V = -3.62\epsilon_F$ and $r_1 = 0.85a$ in equation (4) to pilot inversion. Further optimization leads to $V(r)$ shown in the middle part of figure 6 as the continuous curve. In the superconducting state we invert the tunneling data of McMillan and Rowell [42]. Without normal-umklapp cancellation we let $\delta V = -1.60\epsilon_F$ and $r_1 = 0.37a$ in equation (4) to pilot superconducting state inversion. Further optimization leads to the potential marked by the filled squares in figure 6. With normal-umklapp cancellation we let $\delta V = -3.73\epsilon_F$ and

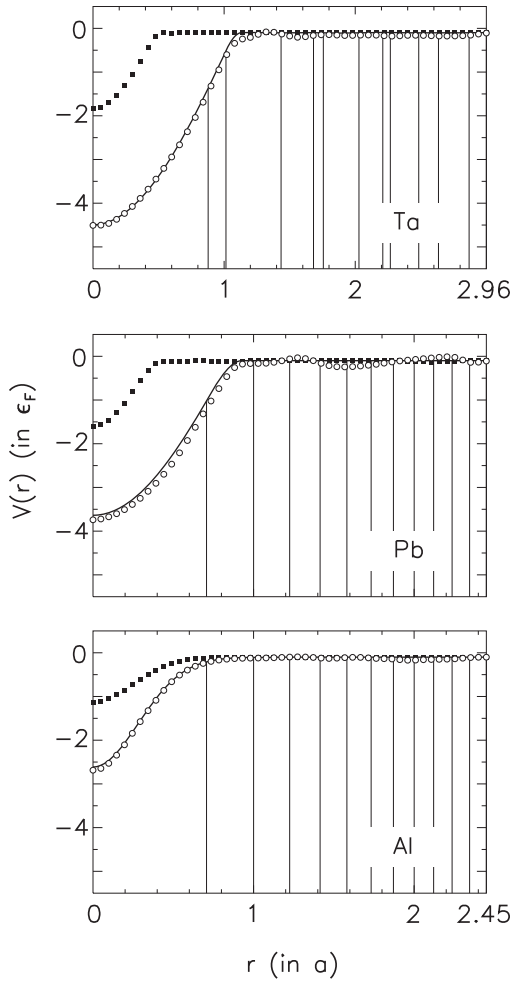

Figure 6. Atomic potentials extracted from Ta, Pb and Al in the normal state (continuous curves) and superconducting state with (open circles) and without (filled squares) normal-umklapp cancellation; conventions identical to figure 3.

Table 1. Superconductor properties with normal-umklapp cancellation

	$2\Delta_0{}^a$	μ^*	$T_c{}^b$	$2\Delta_0/k_BT_c{}^b$
Nb	30.5	0.275	9.23 (9.50)	3.87 (3.80)
Ta	14.0	0.081	4.54 (4.48)	3.58 (3.61)
Pb	27.3	0.150	7.11 (7.19)	4.45 (4.38)
Al	3.40	0.155	1.07 (1.14)	3.67 (3.30)

[a] Experimental value [39], in 10^{-4}eV.
[b] Experimental value [39] bracketed, in K.

$r_1 = 0.88a$ in equation (4) to pilot inversion and find the potential marked by open circles in the middle part of figure 6. On average, when formal normal-umklapp cancellation is introduced, we have 2.53% as the relative difference between the values of $V(r)$, against its depth, in the normal (continuous curve) and superconducting states (open circles).

In the case of aluminum in the normal state we also invert $\rho(T)$ from the Bloch–Grüneisen formula, $\Theta = 395$ K [36]. Here we find the Muffin-tin potential cannot pilot sufficiently accurate inversion. We replace equation (4) with

$$V(r) = \delta V \exp\left[-(r/r_1)^2\right] \tag{6}$$

which is a Gaussian. We let $\delta V = -2.60\epsilon_F$ and $r_1 = 0.39a$ in equation (6) and find $V(r)$ shown as the continuous curve in the lower part of figure 6. In the superconducting state we invert the tunneling data derived from the experimental $\alpha^2F(\nu)$ of Khim [43]. Without normal-umklapp cancellation we let $\delta V = -1.08\epsilon_F$ and $r_1 = 0.35a$ in equation (6) to pilot inversion, giving $V(r)$ shown as the filled squares in the lower part of figure 6. With normal-umklapp cancellation we let $\delta V = -2.67\epsilon_F$ and $r_1 = 0.39a$ to pilot inversion, giving $V(r)$ shown as the open circles in the lower part of figure 6. On average, when normal-umklapp cancellation is introduced, we have 1.02% as the relative difference between the values of $V(r)$, against its depth, in the normal (continuous curve) and superconducting states (open circles).

7. Transition temperature

In each case we have calculated $\alpha^2F(\nu)$ enroute inversion with normal-umklapp cancellation. For the case of niobium it is shown in the lower part of figure 5 as the histogram. Now we calculate T_c by substituting calculated values of $\alpha^2F(\nu)$ into the temperature-dependent Eliashberg–Nambu equations. We start from $T = 0$ and increase T in small steps. We stop calculation when the gap edge drops to less than 1% of its value at absolute zero, Δ_0. We find T_c by extrapolation with a second-order-polynomial. We see from table 1 that calculated values of T_c fit experimental observation to within 3% for three elements. Al with less detailed superconducting tunnelling data as input is off by 7%.

In table 1 we list also values of the Coulomb pseudopotential, μ^*, found enroute inversion with normal-umklapp cancellation and used in our T_c calculation [38]. According to theoretical estimation by Morel and Anderson, based on the Fermi–Thomas approximation, $\mu^* = 0.12$, 0.11, 0.10 and 0.10 for Nb, Ta, Pb and Al, respectively [44] which in some cases differ quite significantly from the values in table 1. On the other hand, according to later and more realistic calculations, $\mu^* = 0.2735$, 0.1169, 0.1446 and 0.1472 for Nb, Ta, Pb and Al [45] which in general are closer to the values in table 1. These are not first principles calculations but come from fitting with tunnelling data, essentially the same method we have been using.

8. Matthias relations

Matthias observed relations between T_c and the number of valence electrons per atom for superconductive metals and alloys but provided no theoretical explanation [46]. In general superconductivity is favored in multivalent systems: T_c peaks at $Z \simeq 4.5$ and 7 but vanishes when $Z \leqslant 2$, $Z = 6$ and $Z \geqslant 8$. The Matthias relations have been widely cited but were considered to be beyond the scope of the BCS theory [3].

With our empirical rule in place the BCS theory can explain at least one aspect of the Matthias relations. In figure 1 the areas between the two grey wedges become larger the larger the valency, allowing more residual umklapp scattering to survive cancellation to contribute to superconductivity and consequently higher T_c. Indeed no $Z = 1$ metal other than lithium ($T_c = 0.4$mK) [47] has been observed to become a superconductor in the ambient.

Metallic hydrogen, $Z = 1$, is widely believed to be an exception. In 1968, based on the perceived high Debye temperature, Ashcroft predicted $T_c = 54.5$ K with the standard weak-coupling BCS expression [48]. In 1989 Barbee III, Garcia and Cohen predicted $T_c \simeq 230$ K with the Eliashberg–Nambu equations and $\alpha^2F(\nu)$ was found without normal-umklapp cancellation [49]. In 2008 Cudazzo *et al* predicted T_c up to 242 K with their novel density functional theory; again $\alpha^2F(\nu)$ was found without cancellation [50]. This escalating T_c in the 40 years from 1968 to 2008 is probably overly optimistic bearing in mind the present insight.

9. Summary and conclusions

We have reconciled the strength of the electron–phonon interaction in metals in the normal and superconducting states. For the superconducting state we start with a simple empirical rule and adhere to it throughout. In it we propose that normal and umklapp scattering cease to contribute to superconductivity when they coexist. Then superconductivity arises solely from residual umklapp scattering in the absence of normal scattering. This empirical rule is without full theoretical justification at present.

Validity of our empirical rule lies chiefly in its capability of extracting virtually identical atomic pseudopotentials for the electron–phonon interaction from not one but four metals in the normal and superconducting states. These are niobium, tantalum, lead and aluminum, thoroughly investigated examples of conventional weak and strong coupling superconductors. Added credibility is gained from the prediction of T_c for each element with good accuracy. Preliminary results for three other metals, molybdenum iridium and tungsten, are equally encouraging. The range of T_c now covered extends from 12 mK to 9.5 K, almost three decades.

To underpin the empirical rule we demonstrate that, when normal and umklapp scattering coexist, the pair occupancy of destination states is doubly defined with conflicting values. We provide an alternative rigorous proof valid in the BCS theory. Apart from being supported by the excellent numerical results in four metallic superconductors, the rule also explains features of the relations observed by Matthias. In light of the rule the high T_c so far predicted for metallic hydrogen is probably overly optimistic. We recognize that further work will be needed to test if the proposed empirical rule can be applied to validate more aspects of the BCS theory quantitatively.

Appendix

The following is a concise and more accessible version of the proof in [30–32]. The BCS reduced Hamiltonian has the following interaction term [1]:

$$-\sum_{\mathbf{k}\mathbf{k}'} V_{\mathbf{k}\mathbf{k}'} b^{\dagger}_{\mathbf{k}'} b_{\mathbf{k}}, \tag{A.1}$$

where $V_{\mathbf{k}\mathbf{k}'}$ measures interaction strength, $\mathbf{k}$ and $\mathbf{k}'$ identify particle momenta while

$$b_{\mathbf{k}} = a_{-\mathbf{k}\downarrow} a_{\mathbf{k}\uparrow} \text{ and } b^{\dagger}_{\mathbf{k}'} = a^{\dagger}_{\mathbf{k}'\uparrow} a^{\dagger}_{-\mathbf{k}'\downarrow} \tag{A.2}$$

with a and $a^{\dagger}$ being the single particle destruction and generation operators. Expression (A.1) can be written as:

$$-\frac{1}{2}\sum_{\mathbf{k}\mathbf{k}'} V_{\mathbf{k}\mathbf{k}'} \left(a^{\dagger}_{\mathbf{k}'\uparrow} a^{\dagger}_{-\mathbf{k}'\downarrow} a_{-\mathbf{k}\downarrow} a_{\mathbf{k}\uparrow} + a^{\dagger}_{-\mathbf{k}'\uparrow} a^{\dagger}_{\mathbf{k}'\downarrow} a_{\mathbf{k}\downarrow} a_{-\mathbf{k}\uparrow} \right). \tag{A.3}$$

Here the first term in the brackets simply is the product of $b^{\dagger}$ and b in expression (A.2). By reversing the signs of the dummy indices $\mathbf{k}$ and $\mathbf{k}'$ (values of $V_{\mathbf{k}\mathbf{k}'}$ not affected) we find the second term. Expression (A.3) highlights that there are two allowed spins for each orbit. This can be seen clearly when we permute the two $a^{\dagger}$'s and two a's in the second term.

Now consider the following scattering event arising from the first term in the brackets of Expression (A.3):

$$(\mathbf{k}\uparrow, -\mathbf{k}\downarrow) \rightarrow \begin{cases} (\mathbf{k}'\uparrow, -\mathbf{k}'\downarrow), & N\text{-process} \\ (-\mathbf{k}'\uparrow, \mathbf{k}'\downarrow), & U\text{-process} \end{cases} \tag{A.4}$$

with the N and U-processes being illustrated by the solid and dashed curved arrows in figure 1, respectively, both arrows start from $\mathbf{k}$. Also consider the event arising from the second term in the brackets:

$$(-\mathbf{k}\uparrow, \mathbf{k}\downarrow) \rightarrow \begin{cases} (-\mathbf{k}'\uparrow, \mathbf{k}'\downarrow), & N\text{-process} \\ (\mathbf{k}'\uparrow, -\mathbf{k}'\downarrow), & U\text{-process} \end{cases} \tag{A.5}$$

when $-\mathbf{k}$ and $-\mathbf{k}'$ are the initial and end states for normal scattering ($-\mathbf{k}$ and $\mathbf{k}'$ for umklapp scattering). Clearly we have identical end states from the N and U-processes in expressions (A.4) and (A.5) respectively. We also have identical end states from the U and N-processes in expressions (A.4) and (A.5) respectively.

In the BCS theory the ground state (trial quasiparticle wave function) must be of the form

$$|\Psi\rangle = \left(\sqrt{1-h_N} + \sqrt{h_N}\ a^{\dagger}_{\mathbf{k}'\uparrow} a^{\dagger}_{-\mathbf{k}'\downarrow}\right)\left(\sqrt{1-h_U} + \sqrt{h_U}\ a^{\dagger}_{\mathbf{k}'\uparrow} a^{\dagger}_{-\mathbf{k}'\downarrow}\right)\left|\Phi\right\rangle \tag{A.6}$$

in order to make expression (A.3) applicable to for example the N and U-processes in expressions (A.4) and (A.5) respectively, h_N and h_U being pair occupation probabilities. Here just two pairs of quasiparticles are generated explicitly, others written collectively as $|\Phi\rangle$. Since $a^{\dagger}_{\mathbf{k}'\uparrow} a^{\dagger}_{\mathbf{k}'\uparrow} = 0$ and $a^{\dagger}_{-\mathbf{k}'\downarrow} a^{\dagger}_{-\mathbf{k}'\downarrow} = 0$, due to double Fermion occupation, we find

from equation (A.6)

$$\langle \Psi|\Psi\rangle = \left[1 - h_N h_U - 2\sqrt{h_N(1-h_N)}\sqrt{h_U(1-h_U)}\right]\langle \Phi|\Phi\rangle \qquad \text{(A.7)}$$

which is not normalized unless h_N or h_U vanishes, consistent with the conclusion in [30–32].

References

[1] Bardeen J, Cooper L N and Schrieffer J R 1957 Theory of superconductivity *Phys. Rev.* **108** 1175–204

[2] Allen P B and Mitrović B 1983 Theory of superconducting T_c *Solid State Phys.* **37** 1–92

[3] Hirsch J E 2009 BCS theory of superconductivity: it is time to question its validity *Phys. Scr.* **80** 035702

[4] Kruchinin S, Nagao H and Aono S 2011 *Modern Aspects of Superconductivity: Theory of Superconductivity* (Singapore: World Scientific)

[5] Carbotte J P 1990 Properties of boson-exchange superconductors *Rev. Mod. Phys.* **62** 1027–157

[6] Zheng X H and Walmsley D G 2007 Asymptotic behavior of Eliashberg gap function in the complex plane and its implications for the Coulomb pseudopotential in superconductors *Phys. Rev.* B **76** 224520

[7] Butler W H, Smith H G and Wakabayashi N 1977 Electron–phonon contribution to the phonon linewidth in Nb: theory and experiment *Phys. Rev. Lett.* **39** 1004–7

[8] Butler W H, Pinski F J and Allen P B 1979 Phonon linewidths and electron–phonon interaction in Nb *Phys. Rev.* B **19** 3708–21

[9] Al-Lehaibi A, Swihart J C, Butler W H and Pinski F J 1987 Electron–phonon interaction effects in tantalum *Phys. Rev.* B **36** 4103–11

[10] Leavens C R and Carbotte J P 1972 Gap anisotropy in a weak coupling superconductor *Ann. Phys.* **70** 338–77

[11] Tomlinson P G and Carbotte J P 1976 Anisotropic superconducting energy gap in Pb *Phys. Rev.* B **13** 4738–44

[12] Truant P T and Carbotte J P 1974 Electron–phonon scattering times for aluminum *Can J. Phys.* **54** 618–23

[13] Tomlinson P G and Carbotte J P 1977 Multiple plane wave calculation of the resistivity of Pb and dilute Pb alloys *Can. J. Phys.* **55** 751–60

[14] Savrasov S Y and Savrasov D Y 1996 Electron–phonon interactions and related physical properties of metals from linear-response theory *Phys. Rev.* B **54** 16487–501

[15] Papaconstantopoulos D A and Mehl M 2002 First-principles study of superconductivity in high-pressure boron *Phys. Rev.* B **65** 172510

[16] Kasinathan D, Kuneš J, Lazicki A, Rosner H, Yoo C S, Scalettar R T and Pickett W E 2006 Superconductivity and lattice instability in compressed lithium from Fermi surface hot spots *Phys. Rev. Lett.* **96** 047004

[17] Yin Z P, Savrasov S Y and Pickett W E 2006 Linear response study of strong electron–phonon coupling in yttrium under pressure *Phys. Rev.* B **74** 094519

[18] Shi L and Papaconstantopoulous D A 2006 Theoretical predictions of superconductivity in alkali metals under high pressure *Phys. Rev.* B **73** 184516

[19] Christensen N E and Novikov D L 2006 Calculated superconductive properties of Li and Na under pressure *Phys. Rev.* B **73** 224508

[20] Lei S, Papaconstantopopoulos D A and Mehl M J 2007 Calculations of superconducting properties in yttrium and calcium under high pressure *Phys. Rev.* B **75** 024512

[21] Nixon L W, Papaconstantopoulos D A and Mehl M J 2007 Calculations of scandium under high pressure *Phys. Rev.* B **76** 134512

[22] Savini G, Ferrari A C and Giustino F 2010 First-principles prediction of doped graphane as a high-temperature electron–phonon superconductor *Phys. Rev. Lett.* **105** 037002

[23] Lüders M, Marques M A L, Lathiotakis N N, Floris A, Profeta G, Fast L, Continenza A, Massidda S and Gross E K U 2005 *Ab initio* theory of superconductivity. I. Density functional formalism and approximate functionals *Phys. Rev.* B **72** 024545

[24] Marques M A L, Lüders M, Lathiotakis N N, Profeta G, Floris A, Fast L, Continenza A and Gross E K U 2005 *Ab initio* theory of superconductivity. II. Application to elemental metals *Phys. Rev.* B **72** 024546

[25] Profeta G, Franchini C, Lathiotakis N N, Floris A, Marques M A L, Lüders M, Massidda S, Gross E K U and Continenza A 2006 Superconductivity in lithium, potassium, and aluminium under extreme pressure: a first-principles study *Phys. Rev. Lett.* **96** 047003

[26] Singh P P 2007 Electronic structure and electron–phonon interaction in hexagonal yttrium by density functional calculations *Phys. Rev.* B **75** 125101

[27] Zheng X H and Walmsley D G 2012 Extracting a more realistic pseudopotential for aluminum, lead, niobium and tantalum from superconductor electron tunnelling spectroscopy data *J. Low Temp. Phys.* **166** 279–97

[28] Zheng X H and Walmsley D G 2013 Evidence for effective weakening of electron–phonon interaction in superconducting tantalum, niobium, lead and aluminum *J. Low Temp. Phys.* **173** 120–42

[29] Hooke R and Jeeves T A 1961 'Direct search' solution of numerical and statistical problems *J. Assoc. Comput. Mach.* **8** 212–29

[30] Zheng X H and Walmsley D G 2004 Umklapp scattering of pairs in BCS superconductivity theory *J. Phys.: Condens. Matter* **16** 8297–309

[31] Zheng X H and Walmsley D G 2005 Coulomb repulsion and T_c in BCS theory of superconductivity *Phys. Rev.* B **71** 134512

[32] Zheng X H and Walmsley D G 2010 122 Renewed look at BCS theory *Renewed Look at BCS Theory in Superconductivity and Superconducting Wires* ed D Matteri and L Futino (New York: Nova) pp 245–70

[33] Pines D 1958 Superconductivity in the periodic system *Phys. Rev.* **109** 280–7

[34] Carbotte J P and Dynes R C 1968 Superconductivity in simple metals *Phys. Rev.* **172** 476–84

[35] Mott N F and Jones H 1958 *The Theory of the Properties of Metals and Alloys* (New York: Dover)

[36] Ziman J M 2001 *Electrons and Phonons* (Oxford: Clarendon)

[37] Webb G W 1968 Low temperature electrical resistivity of pure niobium *Phys. Rev.* **181** 1127–35

[38] McMillan W L and Rowell J M 1965 Lead phonon spectrum calculated from superconducting density of states *Phys. Rev. Lett.* **14** 108–12

[39] Kittel C 1986 *Introduction to Solid State Physics* (New York: John Wiley)

[40] Khim Z G, Burnell D and Wolf E L 1981 Equivalence of optimized conventional and proximity electron tunneling (PET) for niobium *Solid State Commun.* **39** 159–61

[41] Wolf E L, Noer R J, Burnell D, Khim Z G and Arnold G B 1981 Proximity electron tunnelling spectroscopy of Ta: inapplicability of an 'empirical model' *J. Phys. F: Metal Phys.* **11** L23–7

[42] McMillan W L and Rowell J M 1969 Tunnelling and strong-coupling superconductivity *Superconductivity* ed R D Parks vol 1 (New York: Dekker) pp 561–613

[43] Khim Z G 1979 Quasiparticle interference phenomena in thick superconducting Al films, and proximity effects in thin Ag and Al films *PhD Thesis* University of Notre Dame, Indiana
[44] Morel P and Anderson P W 1962 Calculation of the superconducting state parameters with retarded electron–phonon interaction *Phys. Rev.* **125** 1263–71
[45] Mitrović B, Zarate H G and Carbotte J P 1984 The ratio $2\Delta_0/k_BT_c$ within Eliashberg theory *Phys. Rev.* B **29** 184–90
[46] Matthias B T 1955 Empirical relation between superconductivity and the number of valence electrons per atom *Phys. Rev.* **97** 74–6
[47] Tuoriniemi J, Juntunen-Nurmilaukas K, Uusvuori J, Pentti E, Salmela A and Sebedash A 2007 Superconductivity in lithium below 0.4 millikelvin at ambient pressure *Nature* **447** 187–9
[48] Ashcroft N W 1968 Metallic hydrogen: a high-temperature superconductor? *Phys. Rev. Lett.* **21** 1748–9
[49] Barbee T W III, Garcia A and Cohen M L 1989 First-principles prediction of high-temperature superconductivity in metallic hydrogen *Nature* **340** 369–71
[50] Cudazzo P *et al* 2008 *Ab initio* decription of high-temperature superconductivity in dense molecular hydrogen *Phys. Rev. Lett.* **100** 257001